Kinetics of interstitial uptake during gaseous carbo-oxidizing of titanium foils

Kværndrup, Frederik Bojsen; Dahl, Kristian Vinter; Poquillon, Dominique; Ståhl, Kenny; Somers, Marcel A. J.; Christiansen, Thomas Lundin

Published in:
Thermochimica Acta

Link to article, DOI:
10.1016/j.tca.2021.178991

Publication date:
2021

Document Version
Publisher's PDF, also known as Version of record

Thermochimica Acta 703 (2021) 178991

Contents lists available at ScienceDirect

Thermochimica Acta

journal homepage: www.elsevier.com/locate/tca

Kinetics of interstitial uptake during gaseous carbo-oxidizing of titanium foils

Frederik Bojsen Kværndrup [a,*], Kristian V. Dahl [a], Dominique Poquillon [c], Kenny Ståhl [b], Marcel A.J. Somers [a], Thomas L. Christiansen [a,*]

[a] Department of Mechanical Engineering, Technical University of Denmark, DK 2800 Kgs. Lyngby, Denmark
[b] Department of Chemistry, Technical University of Denmark, DK 2800 Kgs. Lyngby, Denmark
[c] CIRIMAT, Université de Toulouse, INP-ENSIACET, 4, allée Emile Monso, BP 44362, Toulouse Cedex 4, Toulouse 31432, France

ARTICLE INFO

Keywords:
Titanium
Thermogravimetry
Diffusion
Kinetics
Microstructure evolution

ABSTRACT

Foils of titanium grade 2 were carbo-oxidized in CO at temperatures ranging from 600 to 1100°C in steps of 50°C. Carbo-oxidation was performed for up to 130 hours in a thermogravimetric setup, enabling the investigation of the kinetics of carbon and oxygen uptake from the gas mixture. The carbo-oxidized specimens were characterized with transmission X-ray diffraction, light optical microscopy, scanning electron microscopy, electron probe microanalysis and nanoindentation to investigate the microstructural evolution along with the uptake of oxygen and carbon. At the surfaces of the foils TiC_x developed, while the core remained h.c.p. titanium. The interstitial content in h.c.p. titanium increased with temperature and first reached its maximum solubility at 1000°C and above. TiO developed within the core for high interstitial contents. The TiC_xO_y phase developed in-between TiC_x and the oxygen containing h.c.p. titanium core for temperatures above 800°C. For temperatures up to 850°C, the uptake of C and O in the titanium foils (initially) obeys a parabolic time dependence. Arrhenius analysis of the thermogravimetry results indicates that volume diffusion of oxygen in h.c.p. titanium is (initially) the rate determining step. For temperatures above 850°C, the activation energy is reduced by a factor 3, suggesting that short-circuit diffusion of species in TiC_x controls mass increase. The hardness of h.c.p. titanium determined with nanoindentation scales with the interstitial content and the associated c/a ratio of the h.c.p. unit cell. The evolution of the microstructure with time and temperature are discussed in relation to the observed kinetics of mass uptake.

1. Introduction

Titanium (Ti) and its alloys are used in applications where high specific strength, corrosion resistance and light weight are essential. However, Ti suffers from inapt tribological properties, thus limiting the use of Ti alloys in applications where wear loads are involved. A remedy can be found in surface hardening, where the dissolution of interstitial elements such as C, N and/or O, in the hexagonal close-packed (h.c.p.) crystal structure of α-Ti and/or the formation of interstitial compounds can enhance the wear performance. This is associated with a substantial increase in strength/hardness as all three elements have a strong solution strengthening effect, albeit with an adverse effect on the ductility, toughness and notch sensitivity [1–3]. Interstitials are an alternative to using Al and V as solid solution strengtheners as in grade 5 titanium, especially concerning biocompatibility of implants, where Al and V potentially can jeopardize health [4]. Surface engineering of titanium for improvement of the tribological properties, can be performed using various methods, which are reviewed and described elsewhere [5,6]. Investigations of the effect of interstitial elements started in the late 1940's addressing the lattice expansion of titanium resulting from incorporation of oxygen (0 – 58 at% O) [7]. During the 1950's the effects of combinations of C, N and O on the mechanical properties were investigated [1,8–10]. In particular, the strengthening effect of interstitial elements was addressed, where one of the conclusions was that nitrogen increases the hardness more than oxygen and carbon. The synthesis of h.c.p. titanium containing oxygen in solid solution has previously been carried out by arc melting in argon of Ti or TiI_4 mixed with TiO or TiO_2, followed by annealing in argon or in vacuum to dissolve titanium oxide and redistribute the oxygen atoms [7,11–13]. In refs. [1,8–10] arc melting of TiI_4 with controlled quantities of TiO_2,

* Corresponding author.
E-mail address: frederikbojsen@gmail.com (F.B. Kværndrup).

https://doi.org/10.1016/j.tca.2021.178991
Received 19 April 2021; Received in revised form 27 June 2021; Accepted 28 June 2021
Available online 3 July 2021

graphite and TiN, followed by annealing in vacuum or argon for homogenization, was applied. It is generally accepted that these interstitials occupy the octahedral interstices in the h.c.p. lattice and lead to an increase of the *c/a* ratio of the lattice parameters [7,13–15]. It should also be noted that interstitial occupancy, *y*, of octahedral sites is a more appropriate terminology than wt% or at. % to describe interstitial solid solutions. The solubility of carbon in α-Ti is roughly 0.4 wt% (y_C = 0.016) at 850°C, while higher contents lead to the formation of NaCl type δ carbide, TiC_x, with x varying from 0.5 – 0.97 [16]. Previous studies suggested that oxygen increases the solubility of carbon in α-Ti [10,17,18], reaching a solubility of 1.5 wt% C ($y_C = 0.061$) with 3.5 wt% O ($y_O = 0.11$) after melting at 1400°C [10]. The solubility of oxygen in α-Ti is 14.1 wt% ($y_O = 0.49$) at 750°C and remains virtually unaltered from 600 to 1750°C [15,19],; higher contents of oxygen lead to a multitude of phases. The expansion of the h.c.p. lattice of α-Ti increases almost linearly with the oxygen content, particularly in the *c* direction of the unit cell [19]. The *c/a* ratio is a sensitive measure for the content of interstitials in α-Ti. The oxide α-TiO_{1-X}, has a wide homogeneity range and – supposedly – exhibits full inter-solubility with the isomorphous compounds δ-TiC_x and TiN_x [20]. The *a* lattice parameter of the δ phase depends on the ratio of C and O contents in the Ti-C-O system. For a carbon occupancy in TiC_x changing from 0.53 to 0.63, *a* increases from 0.430 to 0.432 nm [21]. On the other hand, an increase in O leads to a decrease in *a* from 0.420 to 0.417 nm if the oxygen occupancy in TiO_x changes from y_O=0.637 to 1.275 [15]. Consequently, the occupancies x and y in TiC_xO_y cannot be determined on the basis of X-ray diffraction results only.

The utilization of foils facilitate rapid through-diffusion of interstitial elements and thereby eliminates the sink for interstitials experienced with a *thick substrate* [22]. This allows to identify the microstructural evolution and associated kinetics upon ingress of carbon and oxygen. Here, the Ti-C-O system is investigated in the temperature range 600 – 1100°C, using 25 μm foils and gaseous carbo-oxidizing in an atmosphere consisting of CO, to investigate how the dissociation of CO into C and O affects phase formation in titanium. Dissociation of CO at the foil surface applies both a partial pressure of oxygen (pO_2) and an activity of carbon (a_C). If no equilibrium is achieved between foil and gas, as in a streaming gas, pO_2 and a_C are in principle unknown, but are interdependent, because the temperature is the only adjustable parameter and dissociation of CO provides equal amounts of C and O to the surface. A gas mixture consisting of CO and CO_2 could be applied (Boudouard reaction), which would allow a *controlled*, albeit still interdependent, variation of pO_2 and a_C by adjusting the *ratio* of CO and CO_2 [23]. Preliminary experiments using a gas mixture of 1 vol% CO_2 and 99 vol% CO at 1000°C led to extensive oxidation; for this reason CO/CO_2 gas mixtures were not applied in the present study. Isothermal thermogravimetry of foil specimens in streaming CO gas for a range of temperatures allows the investigation of the overall kinetics of oxygen and carbon incorporation. Additional microstructure characterization provides the microstructural evolution associated with C and O uptake. This insight in the Ti-C-O system is required for optimized and tailored surface engineering of titanium alloys by carbo-oxidizing.

2. Materials and Methods

2.1. Thermochemical synthesis

Annealed grade 2 (G2) titanium foils (GoodFellow) with composition 99.6 wt% Ti, 0.2 wt% O, 0.015 wt% N and 0.15 wt% Fe as reported by the supplier, and a thickness of 25 μm were applied. Foils measuring about 13 × 6 mm^2 were carbo-oxidized in a Netzsch STA449 C Jupiter thermal analyzer in the temperature range 600 – 1100°C at intervals of 50°C using a gas flow of 100 mL/min CO (99.97% purity) and 3 mL/min Ar (99.999% purity) as protective gas. Isothermal thermogravimetry at a range of temperatures provides the overall kinetics of the incorporation of the C and O in the foils. Heating to the carbo-oxidizing temperature was performed at a rate of 20°C/min; cooling to room temperature was performed in the active gas at the maximum cooling rate attainable in the thermal analyzer, approximately 50°C /min. After carbo-oxidizing for 20 - 132 h, the treatment was completed by cooling to ambient temperature in the active gas and flushing with Ar before opening. An overview of reaction temperatures, treatment times and initial sample masses for the eleven samples are given in Table 1. The variation in processing time was partly due to a finite time availability and limitations in the equipment suffering from rapid deterioration of the experimental set-up by high temperature corrosion at high temperatures (1100°C). Even long exposures as 132 h at 1000°C, did not result in reaching a stationary mass; rather very slow reaction kinetics was reached.

2.2. X-Ray diffraction and Rietveld refinement

X-ray diffraction (XRD) analysis was carried out using a Huber G670 diffractometer in transmission (Guinier) mode, using a CuKα1 source. The specimens were fixed at an angle of 45° with respect to the incident beam and rotated about the surface normal to enhance grain statistics and minimize the effect of crystallographic texture. The image strip detector recorded the 2θ range of 3-100° at a step size of 0.005° for an exposure time of one hour. Rietveld refinement of intensity *versus* scattering angle (2θ) was done in WINPOW, which is an modified version of the LHMP program [24], with the purpose of determining lattice parameters, phase fractions and zero shift corrections. The latter is a correction for possible horizontal shifts of the foils during measurement due to bending. The peaks were fitted with pseudo-Voigt functions, while the background was fitted with Chebyshev polynomials. Texture corrections for the (110) and (011) reflections were used to improve the refinement, however due to the textured nature of the foil, it is not feasible to achieve a perfect fit of the measured intensities. Goodness-of-fit values $\chi^2 \leq 4.15$ and residual values of $R_p \leq$ 2.66% were achieved, with difference curves of low intensity, demonstrating insignificant differences between the measured and calculated diffractograms. LP values for the α and δ phases had minor standard deviation values below 10^{-4} nm.

2.3. Microscopical investigation

Pieces of the carbo-oxidized foils were cold embedded in epoxy, ground and polished, using sequentially finer sandpaper down to #4000, followed by 3 and 1 μm diamond suspensions, and finally basic 0.3 μm colloidal silica suspension as the final step for 2 minutes. Leftover silica particles were removed with ultrasound. Etching was done on the 700 – 1000°C specimens, with Murakami's reagent (10 g sodium hydroxide, 10 g potassium ferricyanide and 100 mL water) at 55°C for 3.5 minutes in order to reveal the carbides. Light optical microscopy (LOM) was performed on the cross sections with polarized light on a ZEISS Axio Vert.A1 at 50x magnification. Scanning electron microscopy (SEM) and energy-dispersive X-ray spectroscopy (EDS) on carbon-coated non-etched cross-sections of the 650, 850 and 1100°C foils were performed on a Zeiss Supra 35 FEGSEM using 20 kV acceleration voltage, a 30-μm aperture size in back scatter electron (BSE) imaging mode.

Table 1
Treatment scheme for the carbo-oxidation of G2 titanium foils at 600 – 1100°C with CO and Ar.

T /°C	t / h	T /°C	t / h
600	89	900	94
650	100	950	100
700	91	1000	132
750	69	1050	91
800	100	1100	20
850	100	–	–

2.4. Chemical analysis

Determination of the total absorbed carbon content in the specimens was achieved on a CS230 LECO Carbon/Sulfur Determinator using LECO iron chip accelerant and Lecocel II. A steel containing 0.807 wt% C (LECO standard - 502-893) was used for calibration of the instrument. Quantification of the carbon content by this technique is based on total combustion of the specimen and conversion of C into CO_2. The content of CO_2 in the resulting gas is measured with infrared spectrometry.

Oxygen and carbon concentration profiles were measured on cross sections of the embedded 750, 850 and 1100°C samples by electron probe micro analysis (EPMA) with a CAMECA SXFive FE microprobe working at 10 kV and 20 nA. For the chosen conditions, the volume analyzed is estimated at 1 μm^3. Samples were polished just before the analyses in order to limit surface contamination. Two profiles were determined with a step size of 1.5 μm over the cross sections of the selected foils. For quantification, the following reference materials were used: SiC for C, Fe_3O_4 for O, pure Ti for Ti and pure Fe for Fe.

2.5. Nanoindentation

Nanoindentations were performed on cross-sections of the foils applying a diamond Berkovich indenter on a NHT^2 nano-indenter from CSM Instruments. A constant load of 40 mN with a varied indentation depth between 400 and 900 nm was achieved; the holding time at peak load was 5 seconds. Hardness values were obtained from the indentation data, using the method due to Dao et al. [25]. For this purpose on average 50 validated indents were performed in the center of the foils along multiple grains and orientations (for a detailed description of the procedure see [26]). The indentation results were calibrated on fused silica an integrated into the quantification method. The loading/unloading parts of the load-displacement curves were examined for discontinuities/anomalies, which would suggest grain boundaries or crack formation [27]. Indentations affected by the vicinity of a grain boundary, porosities or a crack were excluded from the data presented.

3. Results

3.1. Thermogravimetric analysis

The total mass gain, Δm, relative to the initial foil mass, m_o, associated with uptake of carbon and oxygen from the gas in the foil as recorded with thermogravimetric analysis (TGA), is given in Fig. 1 for the foils treated in the temperature range 600 – 1100°C. Apparently, there is a difference between the mass gain curves for temperatures below 850°C and those from 900°C and above, as reflected by the relatively large additional mass gain from 850 to 900°C. This temperature range contains the α → β transition at 882°C [19]. In order to identify the cause for this "gap", the first part of mass gain curves is shown in Figs. 1B and C. For the mass gain curves in the range 600 – 700°C a parabolic time dependence applies for the entire curves (see Fig. 1 (B)); an analogous parabolic mass gain is observed for the initial part of the curves for 750 - 850°C; the duration of the parabolic stage is shorter the higher the carbo-oxidation temperature. The parabolic time dependence strongly suggests diffusion-controlled uptake of species from the reactive gas [28]. For temperatures from 900°C and above, no parabolic mass gain was observed. Rather, the mass uptake accelerated rapidly in the initial stage and declined continuously according to a non-parabolic dependence after a relatively short time.

3.2. Transmission X-ray diffraction

Transmission XRD patterns of the synthesized foils and the untreated reference foil are given in Fig. 2. The untreated reference consists of α-Ti and has a weak 010 texture, while the carbo-oxidized specimens are converted into a solution of interstitials in α and δ phase, i.e. TiC, TiCO

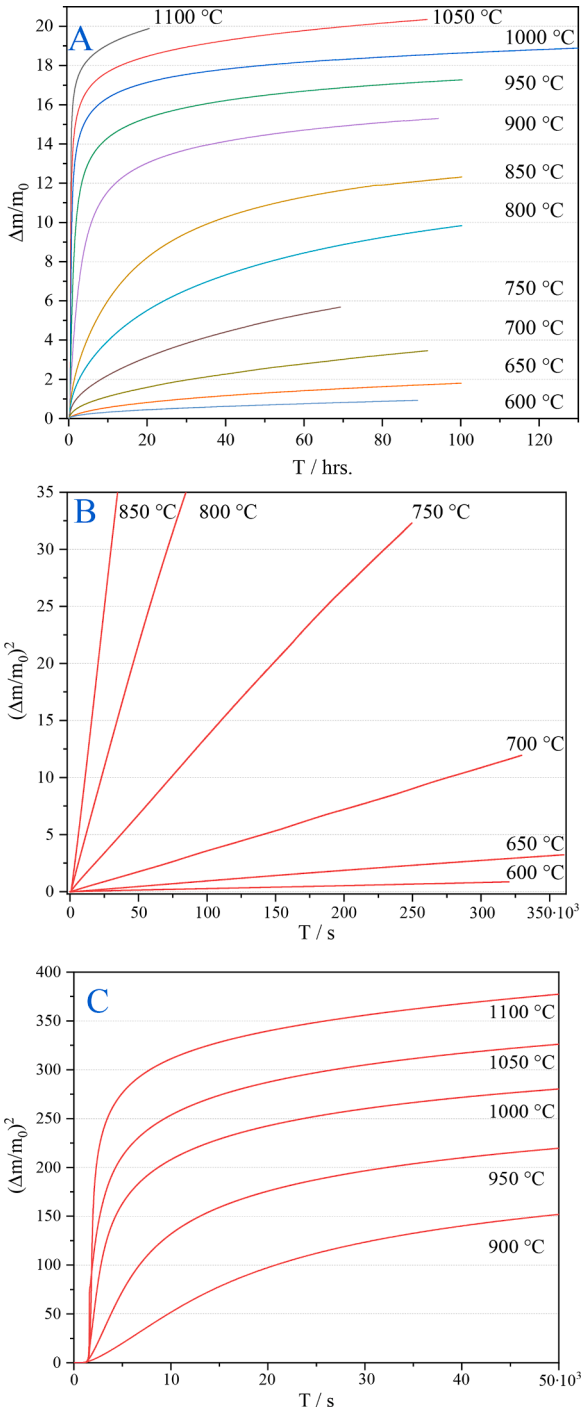

Fig. 1. Relative mass gain curves (thermogravimetry) for the carbo-oxidized G2 titanium foils at temperatures ranging from 600 to 1100°C in CO for 20 – 132 h. In (A) the mass uptake relative to the initial mass is given for all experiments. In (B) the square of the relative mass increase is given as a function of t for temperatures up to 850 °C and from 900 °C in (C). The kink in the 1050°C curve is caused by a brief loss of connection with the thermal analyzer.

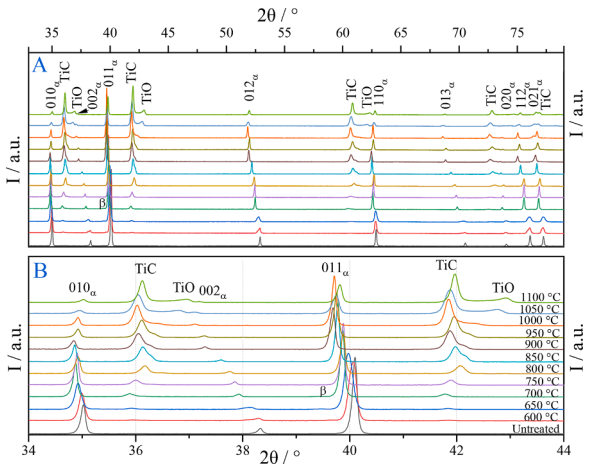

Fig. 2. Transmission X-ray diffractograms for the carbo-oxidized and untreated G2 titanium foils. A) full range from 33 to 79. B) Subset of A showing the range from 34 to 44°; the annotations and color coding apply for both figures. Detected phases are h.c.p. α-Ti, δ-TiC (high C content), δ-TiCO, δ-TiO (high O content) and the Fe stabilized β phase for 600 – 700°C.

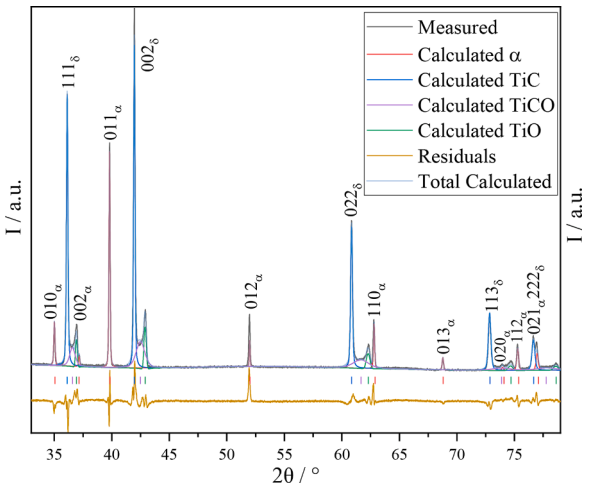

Fig. 3. X-ray diffraction pattern, refined Rietveld profile and residuals curve for 33 – 79° 2θ (full range is 3 – 100° 2θ) for the 1100°C sample. Vertical lines mark Bragg positions for the different phases.

and TiO with an f.c.c. sublattice of Ti atoms; no indications for the presence of TiO_2 or Magnéli phases was observed[1]. It is not possible to quantify the C and O contents in these mixed interstitial phases from XRD alone (see Introduction). The peak at 39° 2θ for the 600 – 700°C specimens is identified as b.c.c. β-Ti that is stabilized by an Fe impurity in the alloy. The α-Ti peaks that are most sensitive for a change in the *c* lattice parameter of the h.c.p. lattice, such as the 002 peak at 38° 2θ and the 012 peak at 52° 2θ, exhibit a pronounced shift to lower 2θ values with increasing reaction temperature, indicating a lattice expansion in the *c* direction and thus an increase in the *c/a* ratio. The *a* lattice parameter is only affected slightly by the incorporation of oxygen and carbon. The α-Ti peaks at 600 and 650°C are asymmetrically broadened towards lower diffraction angle, suggesting the presence of compositional variation over the diffracting volume; above 700°C peak asymmetry is no longer encountered. The intensities of the δ (TiC_xO_y) peaks increase with reaction temperature, along with a reduction of the intensity of the α-Ti peaks, indicating a transformation of α into δ (TiC_xO_y). The 800 – 1100 °C specimens contain satellite peaks and asymmetries to the high 2θ side of the TiC peaks, which suggests that a mixed interstitial phase TiCO develops. A new TiO peak is also detected at even higher 2θ for the 1050 and 1100 °C specimens; the higher 2θ the higher is the O content in the δ phase.

Rietveld refinement of the diffractograms provided the weight fractions of the phases present as well as the lattice parameters of the phases. By means of example, the refined Rietveld profile for the 1100°C is presented in Fig. 3 and contains the phases/structures α-Ti and the δ phases with various C and O contents and denoted as "TiC", "TiCO" and "TiO". This is the most complex diffractogram of the investigated series, because significant overlap of peaks of the various phases occurs. From the residuals curve it is clear that the fit is successful; similar and, generally, better fits were obtained for the other specimens. For most specimens, the 012_α peak lacks intensity, which is attributed to crystallographic texture in the foils. It was not possible to fully correct for the presence of texture by use of, arbitrary, texture correction factors. As a consequence, the phase fractions of α-Ti are underestimated, especially for the 600 – 800°C specimens. The rather wide and low-intensity peak in-between the TiC and TiO peaks in Fig. 3, indicates a broad variation in the C and O contents in TiC_xO_y, and is therefore fitted as a peak enveloping the "TiCO" phase.

The results from the Rietveld refinements are collected in Fig. 4 and

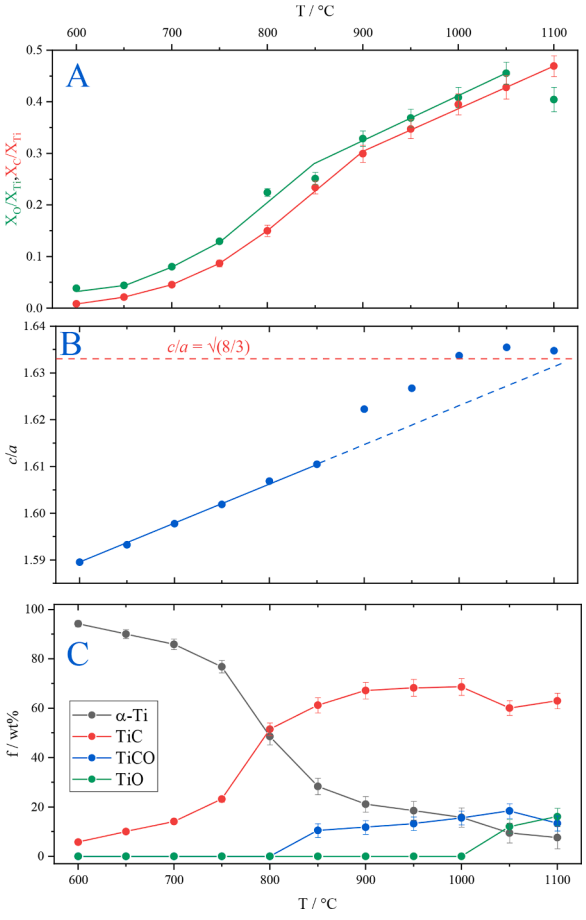

Fig. 4. (A) Molar fractions of C and O relative to the molar fraction of Ti, calculated based on total uptake in TGA and carbon determination experiments. (B) The *c/a* ratio of h.c.p. α-Ti. Estimated standard deviations are too small to be visible. (C) Phase fractions (wt%) as obtained by Rietveld analysis. δ phases are slightly overestimated, due to texture effects for the α phase, which is reflected by the standard deviations.

[1] The TiC, TiCO and TiO phases have a NaCl type crystal structure and are referred to as δ-phase, containing both C and O, a more precise terminology would be TiC_xO_y with known x and y values, however the calculation of these values is not possible solely on the basis of XRD results (see Introduction), making this terminology an approximation.

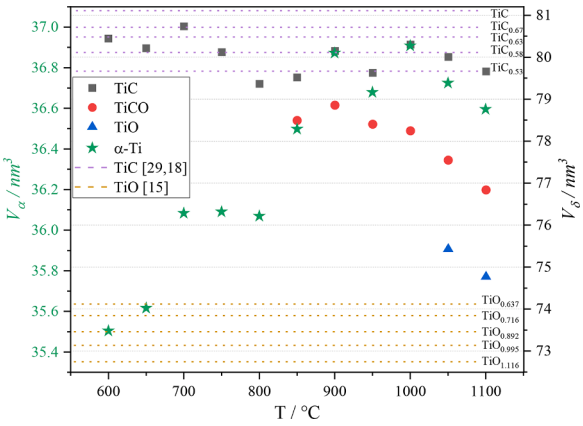

Fig. 5. The volume of the unit cell for TiC, TiCO, TiO and h.c.p. α in comparison with literature values for TiC [29], $TiC_{0.67\text{-}0.53}$ [18], and $TiO_{0.637\text{-}1.116}$ [15]. Estimated standard deviations are too small to be visible on the presented scale.

Fig. 5; Fig. 4 contains the evolutions of *c/a* ratio of h.c.p. Ti and the phase contents along with C and O contents, while Fig. 5 provides the volumes of the unit cells for NaCl-type phases and h.c.p. Ti. From the phase fractions it is evident that initially h.c.p. Ti is dominant, while for temperatures above 800°C TiC_x becomes the dominant phase. The phase contents of TiO_x and TiCO do not exceed 20 wt%.

The *c/a* ratio increases linearly with treatment temperature up to 850°C. Above this temperature an additional increase in *c/a* ratio occurs and eventually at 1000°C a plateau is reached just above the ideal *c/a* ratio ($=\sqrt{8/3}$) for h.c.p. lattices. The progressive increase in *c/a* ratio until a plateau is reached indicates that the total interstitial content in h.c.p. Ti increases with reaction temperature and that saturation of the h.c.p. phase with interstitial atoms (mainly oxygen) is not reached in any of the specimens carbo-oxidized at a temperature below 1000°C. It is recognized that a change in ratio between the interstitial elements could lead to a change of the *c/a* ratio, because carbon expands α-Ti more than oxygen, as reported for very low contents of C and O [1]. This is considered a minor effect in the present context, because the maximum solubility of C in h.c.p. Ti is very small as compared to the maximum solubility of O.

From the unit cell volumes for the δ phases in Fig. 5 it is evident that neither TiC nor TiO is stoichiometric. It is noted that the unit cell volume of δ depends on both the total interstitial content present in the f.c.c. Ti sublattice as well as on the actual octahedral site occupancies of C and O. For a synthesis temperature in the range 600 – 750°C the observed unit cell volumes for TiC are consistent with TiC_x for x=0.58-0.63, while for a higher synthesis temperature x=0.53-0.58. This might be consistent with a larger carbon deficiency with increasing temperature, as observed in the Ti-C phase diagram, but it may also indicate that oxygen is dissolved in TiC_x (in addition to, or as a substitute for, C), because oxygen reduces the lattice parameter (cf. the data for $TiO_{1\text{-}x}$ in Fig. 5).

The *overall* contents of C and O expressed as the molar fractions of C and O divided by the molar fraction of Ti in the synthesized materials as determined by TGA and LECO carbon analysis are presented in Fig. 4 (A)[2]. The contents of C and O increase progressively with reaction temperature. For the lower treatment temperatures more oxygen than carbon appears to be incorporated in the foils, while from 850°C it is observed that C:O=1:1, apart from a slight decrease in oxygen content for the 1100°C sample. Furthermore, from 850°C the dependence of incorporated O and C on treatment temperature is linear.

[2] The total weight gain from TGA is equal to the C + O content, while LECO measures the C content.

3.3. Light optical and scanning electron microscopy

The temperature evolution of the microstructure in the carbo-oxidized Ti-foils as investigated with LOM is presented in Fig. 6, while selected SEM BSE micrographs are provided in Fig. 7. The microstructure consists of a surface layer on both surfaces of the foil denoted "TiC" phase, an intermediate phase denoted "TiCO" phase and a core of an interstitial solution in α-Ti (cf. XRD). Substantial grain growth occurs in the α-Ti phase. The difference in grey tone between α-Ti grains is a consequence of using polarized light, which leads to contrast differences between differently oriented grains in h.c.p. Ti, associated with different thicknesses of native oxide. The notably darker interphase layer in the 800 – 1100°C foils, developing in-between the outer TiC and inner α-Ti shows the presence of another phase that responds differently to Murakami's reagent than TiC. For the 950 – 1100°C foils, the α-Ti phase in the core contains oriented plates (Fig. 6 and Fig. 7), which indicates a preferred orientation relationship with the h.c.p. α-Ti grains and the developing phase. The plates are interpreted as the TiO phase with a high oxygen content that appear in the 1050 – 1100°C foils (cf. Fig. 4 (C); for temperatures below 1050°C it was not possible to quantify the low content of TiO with XRD). These plates developed within the α-Ti phase saturated with O (cf. *c/a* ratio in Fig. 4 (B) and EPMA profiles in Fig. 8). Since, the TiO phase has an f.c.c. sublattice of Ti atoms and saturated h.c.p. Ti has a near-ideal *c/a* ratio, it is suggested here that h.c.p. Ti(O) transforms easily into NaCl TiO by the introduction of stacking faults, whereafter more O can be accommodated. An analogous transformation was recently identified for TiH_2 formation in Ti and dubbed pseudo-martensitic [30], because the Ti sublattice transforms by a martensitic mechanism, whereafter interstitials occupy the interstices in the f.c.c. Ti host lattice by diffusion; in this sense the overall transformation is not diffusionless and, hence, pseudo-martensitic. The 600 – 700°C foils contain additional distinctive microstructural features as plates and "speckles" in the core of the foils (Fig. 6 and Fig. 7). For the 650°C foil, these were further investigated with transmission electron microscopy and identified as δ-TiH_2 phase with a f.c.c. sublattice of Ti atoms (see [31] and [32]). Initially, the H content in the foils is only 60 ppm. Subsequent H uptake from trace amounts of H in the CO or Ar gasses during heating cannot be ruled out.

The light phase observed in the BSE micrographs (Fig. 7) contains iron that is present in the foils as an impurity and is identified as β-Ti (b.c.c.), which is stabilized by the presence of iron. Iron is a very mobile alloying element in titanium and, correspondingly, has a diffusivity that is nearly one order of magnitude larger than the interstitial diffusivity of oxygen [33]. The accumulation of iron in the center of the foil is therefore thought to be a consequence of the ingress of the strongly α-stabilizing O atoms, which pushes ahead the iron atoms and thus the distribution of β-phase to the interior of the foil (cf. micrographs at 600 - 700°C in Fig. 6). The disappearance of β-phase may provide an explanation for the significant grain growth following the CO treatment, as β-phase no longer pins the positions of the α grain boundaries. An analogous argumentation applies for the concentration of TiH_2 in the core: H, originally present in the foils, is pushed ahead of the ingressing oxygen. Since oxygen enhances the solubility of H in h.c.p. Ti, and the O content increases with temperature, TiH_2 will eventually disappear.

The small bright regions observed in the TiC_x layer along the foil surfaces and visible from 750°C (Fig. 6) coincide with the black regions in Fig. 7b/c and are interpreted as porosities that have developed in TiC_x. The TiCO layer in-between TiC_x and the core is not porous.

3.4. Electron probe microanalysis

The contents of O and C determined with EPMA along lines across the foil thickness are given Fig. 8 for three selected specimens. For each foil, two lines, denoted as #1 and #2, are given. Average interstitial occupancies, y_C and y_O, of C and O, respectively, within TiC, TiCO and α-Ti phases are given in Table 2. The composition profiles in Fig. 8 show

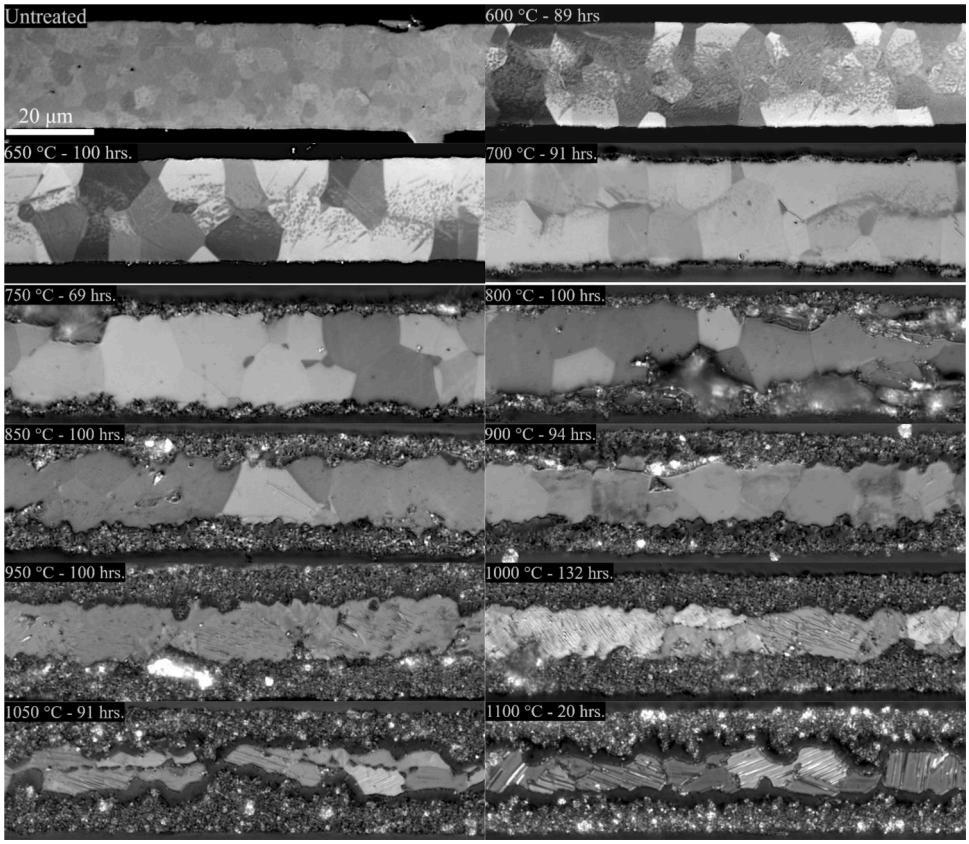

Fig. 6. Polarized light micrographs of non-etched (untreated, 600 and 650°C) and Murakami etched (700 – 1100°C) cross-sections of the thermochemically treated foils (CO and 600-1100°C). The microstructures contain an outer TiCO compound layer and a core consisting of expanded h.c.p. α phase. The scale bar given for the untreated reference applies for all micrographs. The bright parts are polarized light effects.

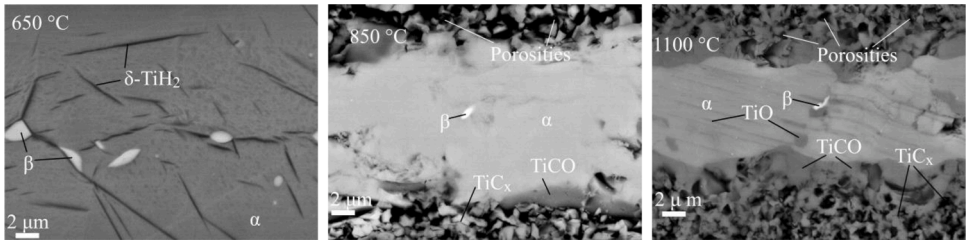

Fig. 7. Backscatter electron micrographs in the cores of the foils carbo-oxidized at 650, 850 and 1100°C (left to right) foils.

that the interstitial contents in the α-Ti core are uniformly distributed; no composition gradients occur, in agreement with the sharp peaks for α-Ti in Fig. 2. Evidently, the amount of O dissolved in α-Ti increases pronouncedly with the synthesis temperature, consistent with the increase in *c/a* ratio (Fig. 4 (B)). Along with this increase in O content, the C content increases, too. The O content reaches a maximum of $y_O = 0.61$ at 1100°C, which is higher than the previously reported maximum of $y_O = 0.49$ [19]. This high content is in agreement with the presence of TiO in addition to h.c.p. Ti in the core. The TiC_x layer at 750°C (cf. XRD, LOM and SEM) is identified as $TiC_{0.86}O_{0.07}$. At 850 and 1100°C the contents of C are lower, while the O contents are higher, resulting in the compositions $TiC_{0.82}O_{0.21}$ and $TiC_{0.72}O_{0.34}$, respectively. Within experimental accuracy these compositions equal a 1:1 ratio of metal and interstitial atoms; if an over-stoichiometric content of interstitials is present, this could be explained by the presence of vacancies on the Ti-sublattice. The TiCO layer, which is most clearly observed for the 1100°C foil in Fig. 6 and Fig. 7, reaches a composition $TiC_{0.30}O_{0.63}$.

3.5. Nanoindentation

The hardness and indentation modulus as a function of the *c/a* ratio of α, as obtained by nanoindentation, are given in Fig. 9 (A) and (B). The *c/a* ratio increases linearly with interstitial content and allows for a comparison between reaction temperatures. The hardness displays a linear dependence on the *c/a* ratio up to 850°C, while the hardness increases sharply at 900 – 1100°C, due to the inherent hardness of the TiO phase. The indentation modulus displays a similar linear increase with *c/a* ratio, although there is a slight decrease at low content, which is due to the slight contraction in *a* [26]. The TiO phase also strongly increases the indentation modulus. From 600 to 850°C the hardness and indentation modulus display similar increases with the *c/a* ratio as presented in [26], and suggest that the interstitial content at 900 – 1100°C is higher or close to the maximum y_O content from literature ($y_O = 0.5$ [19]). The effect of anisotropy and difference in grain orientation is reflected by the standard deviation, while the effect of the TiO plates inside the α-Ti grains from 900 – 1100°C, leads to a sharp increase in standard deviation, because both phases are measured simultaneously,

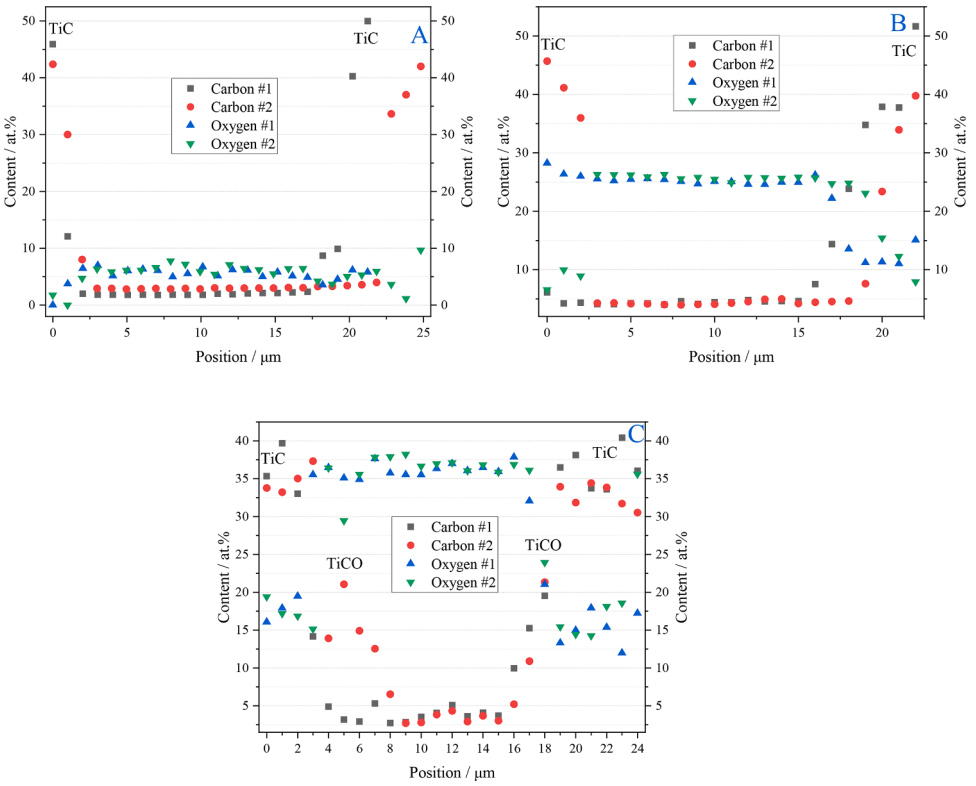

Fig. 8. EPMA line profiles of O and C along 2 lines across the foil thickness for 750°C (A), 850°C (B) and 1100°C (C).

Table 2
Average compositions of the TiC layer, α-Ti core and intermediate "TiCO" phase.

	TiC		TiCO		α-Ti	
T /°C	y_O	y_C	y_O	y_C	y_O	y_C
750	0.07±0.03	0.86±0.04	0.12±0.01	0.05±0.01	0.07±0.01	0.03±0.01
850	0.21±0.03	0.83±0.05	0.31±0.06	0.27±0.08	0.36±0.01	0.06±0.01
1100	0.34±0.02	0.72±0.03	0.63±0.06	0.30±0.04	0.61±0.01	0.07±0.01

but to different degrees in differently oriented grains. There is a slightly increased tendency for crack formation for the high temperature samples, caused by the lower ductility at higher interstitial content. The force-displacement curves are given in Fig. 9 (C) and (D), and show that the increasing interstitial content leads to a reduction in displacement from about 850 nm to about 380 nm at a constant load of 40 mN.

4. Discussion

4.1. Reaction kinetics

The dissociation of CO at the foil surface results in equal contents of adsorbed C and O species at the surface; adsorbed C/O can enter into solid solution. Alternatively, C can stay at the surface and form C-species as for example graphite, while O can react with CO from the gas under formation of CO_2. Carbon dissolved in the solid state is generally not able to leave the material by reaction with CO, unless water vapour is applied. As follows from Fig. 4 (A), C and O are taken up to approximately the same extent, irrespective of temperature, indicating that no soot formation occurred, nor the removal of oxygen by the Boudouard reaction at the surface. Upon exceeding the limited solubility of carbon in Ti, irrespective of whether it is h.c.p. or b.c.c., close to the surface, the TiC phase nucleates. For O the solubility in α-Ti is very high, so much more O than C can be accommodated in solid solution before the solubility limit is reached and there would be a driving force for the formation of Ti-oxide.

The uptake of C and O in the Ti-foils is coupled since both are provided in equal contents at the surface. If the uptake of one of the components is rate determining, it has consequences for the rate of uptake of the other species and the amount of CO that dissociates at the surface. The observation of parabolic mass increase in Fig. 1 for synthesis temperatures up to 850°C strongly suggests that diffusion of (one of the) interstitial species is rate determining. Considering that (the initial part of) the mass uptake curves follow a relation $\left(\frac{\Delta m}{m_o}\right)^2 = K \cdot t$, with K the parabolic proportionality constant, it is obtained that K follows an Arrhenius type expression (Fig. 10 (A)) with an apparent activation energy of $Q_{app} = (199.3 \pm 4.6)$ kJ.mol^{-1}. This value is identical, within experimental accuracy, to the activation energy for oxygen diffusion in h.c.p. Ti: $Q = 200$ kJ.mol^{-1} [33]. For the lowest synthesis temperatures, 600 - 700°C, parabolic mass increase was observed for the entire synthesis curve and XRD indicated the presence of composition gradients in α-Ti at the end of the chosen synthesis time. For synthesis temperatures 750 - 850°C parabolic mass increase was observed in the initial stage, while no composition gradients were observed in h.c.p. Ti at the end of the synthesis time, and uniform composition distributions over the h.c.p. Ti core of the foil (Fig. 8 (A/B)). Hence, in the 750 - 850°C range, the transition from parabolic mass uptake in the initial stage to slower kinetics is interpreted as levelling out of composition variations in the h.c.p. Ti phase and transition to another rate determining step. Even though there is no composition gradient in the core of foils carbo-oxidized above

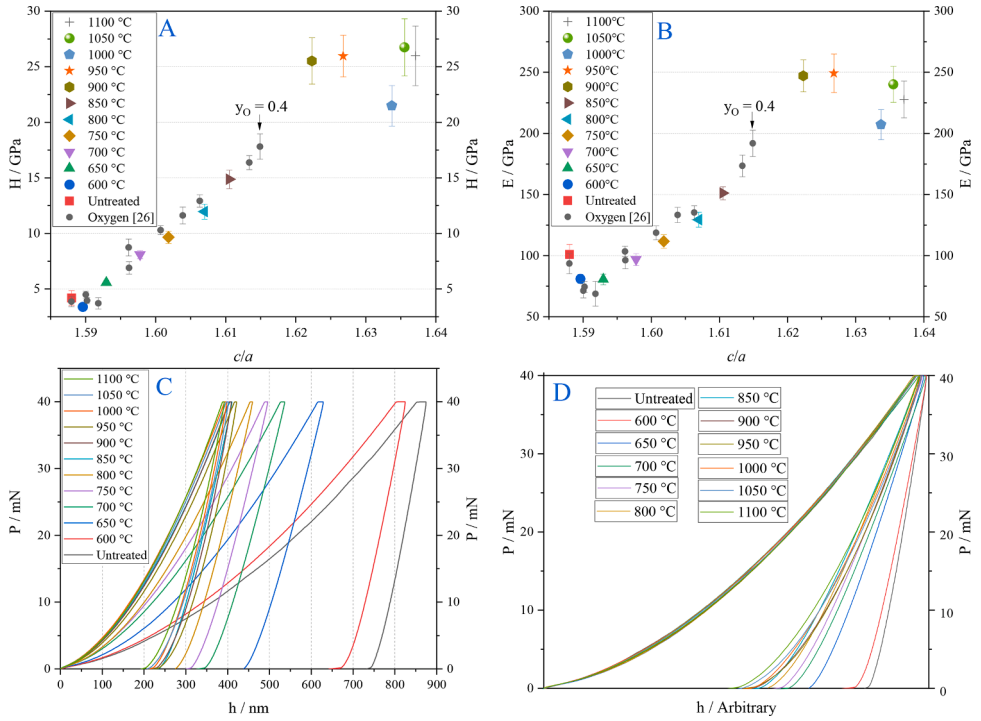

Fig. 9. (A) Hardness vs. *c/a* ratio and indentation modulus (B) compared with literature data. (C) show the averaged force-displacement curves based on around 50 indents per. Sample (D) display the force-displacement curves with arbitary displacement.

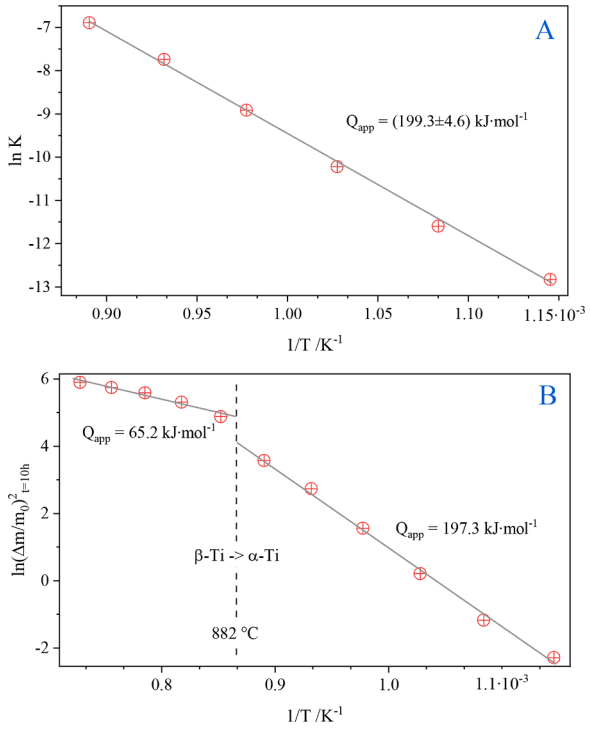

Fig. 10. (A) Arrhenius presentation of the parabolic proportionality constant K for synthesis temperatures up to 850°C; (B) Arrhenius presentation of the mass uptake after 10 h showing two kinetic regimes which appear to change at the α→β transition temperature.

700°C, the h.c.p. Ti phase is not saturated with interstitials as reflected by the *c/a* ratio in Fig. 4 (B). Overall, the experimental results are consistent with diffusion-controlled uptake of both C and O in the foils, where the rate-controlling step is diffusion of O in α-Ti. This is further corroborated by DICTRA [34] simulations of the oxygen composition profile over a 25 μm thick Ti foil with an initial 0.6 at.% O and a constant (but temperature dependent) surface concentration (see Supplementary material Fig. S1). It is noted that diffusion control by oxygen diffusion in h.c.p. Ti does not imply that no TiC layer can be present (consistent with Fig. 2 and Fig. 4); neither does it imply that TiC does not grow. It only means that mass uptake in the entire foil is dictated by oxygen diffusion in α-Ti, the slowest step in the chain of transport mechanisms. Upon its nucleation in an early stage, the TiC layer grows into the Ti-foil, implying that transport of C and O through TiC to the interface between TiC and the Ti-core is necessary to establish this growth. Diffusion of carbon through a film of TiC thicker than 20 nm leads to a growth rate that is inversely proportional to the film thickness [28], i.e. parabolic, provided that C diffusion through TiC is the rate determining step. If diffusion of O in h.c.p. Ti is the rate determining step in the overall mass uptake, it implies that transport through the TiC layer is, compared to this, rapid albeit parabolic, and determined by the amount of C (and O) incorporated. Carbon (and oxygen) would diffuse through TiC by an octahedral vacancy mechanism, suggesting that the higher the concentration of vacancies on the interstitial sublattice, the faster can diffusion through the TiC layer proceed. The diffusion of carbon in TiC was found to depend strongly on TiC stoichiometry, such that the diffusion coefficient increases with increasing carbon deficiency [35]. The effect of Ti vacancies on diffusion in TiC is considered negligible since it amounts to ~ 0.5 % [36]. In this respect, it is not surprising, that the highest carbon content in TiC is observed for the lowest synthesis temperatures, because the supply of C is sufficient to maintain a relatively high interstitial content. The self-diffusion coefficient of carbon in TiC is larger than that of oxygen [37]. The observation that the TiCO phase develops in-between TiC and the oxygen containing α-Ti core in the foils for synthesis temperatures above 800°C is likely to be associated with this. After the diffusion of O in h.c.p. Ti is no longer the rate-determining step, the O that is transported through the TiC layer is no longer incorporated entirely in the core, thus leading to accumulation in TiC (cf. Table 2 which shows indeed that the O content in TiC increases from 750 to 850°C) and TiCO formation, as detected with XRD. Along with an

increase in synthesis temperature, the oxygen content in TiCO increases, as follows from the reduction in lattice parameter (cf. Fig. 5).

For synthesis temperatures above 850°C no parabolic mass uptake was observed, but rather a rapid acceleration followed by a gradual deceleration. In this temperature range diffusion of O in α-Ti proceeds rapidly already during heating to the synthesis temperature. The transition of α-Ti into β-Ti during heating above β-transus implies that initially, and this can be short, O diffuses into β-Ti, wherein the diffusivity for O is higher than in α-Ti, about 10^{-12} $m^2 \cdot s^{-1}$ and 10^{-13} $m^2 \cdot s^{-1}$ at about 900°C, respectively [33]. The oxygen-induced conversion of β-Ti into α-Ti implies a fast increase in O content (during heating), while the homogeneity range in α-Ti is narrower as compared to lower T, because an α-Ti layer grows into β-Ti. Both these conditions imply that faster than parabolic mass uptake is possible, which would explain the observed kinetics in Fig. 1. Also, the total interstitial content that is obtained in α-Ti can be higher than the linear dependence on synthesis temperature in the 600 - 850°C range.

In order to compare the kinetics in the 850 - 1100°C range with that in the 600 - 850°C range, the mass uptake after 10 h is compared in Fig. 10 (B). Firstly, the apparent activation energy for the low temperature range is identical, within experimental accuracy, with that in Fig. 10 (A) from the parabolic proportionality constant, thus validating this approach. Secondly, the apparent activation energy in the high temperature regime is lower by a factor 3. It is unknown whether this value can be attributed to a specific rate-determining step. Recognizing the low value of the apparent activation energy, it is suggested that short circuit diffusion, e.g. along grain boundaries, of C/O through the TiC layer controls the overall mass uptake, recognizing that the diffusion coefficients of C and O through TiC at 1000°C are of the order of 10^{-14} and 10^{-16} $m^2 \cdot s^{-1}$, respectively [35,37]. It is remarked that the presence of porosity in the TiC_x layer can provide a mechanism for CO transport if the porosities are interconnected with the externally supplied CO. Extrapolation of the Arrhenius dependence from the high-temperature regime with Q_{app}= 65.2 $kJ.mol^{-1}$ to the low-temperature regime shows indeed that the mass uptake that would have been realized if transport through TiC were rate determining is appreciably higher than accomplished by O-diffusion in the core as the rate-determining step. Vice versa, in the high temperature regime oxygen diffusion in h.c.p. Ti can accomplish faster mass uptake than transport through TiC.

4.2. Microstructural evolution in the foils

A schematic representation of the growth kinetics for 650, 850 and 1100°C is given in Fig. 11. The foils initially contain small grains of α-Ti with small β-Ti particles/regions randomly dispersed (cf. Fig. 6). Synthesis at 650°C initially forms a thin layer of TiC_x; transport of C and O through this thin layer is accomplished by short circuit, grain-boundary, diffusion. The oxygen concentration profile is indicated as red dotted lines (cf. Fig. S1), and illustrates how the 650°C foil retains a wide concentration gradient even after 100 hours of treatment. The reason for this is the slow volume diffusion of O at this temperature. The diffusion of oxygen into α-Ti also drives the Fe-rich β particles (white) into the center. The β particles limit grain growth of α-Ti at lower temperature, by pinning the grain boundaries; this effect subsides at temperatures above the α→β transition temperature of 882°C in commercially pure titanium [38]. It may be suggested that the observed grain growth alters the kinetics of oxygen ingress into α-Ti, because the density of grain boundaries is reduced with time. Generally, the effect of grain boundaries on the kinetics of interstitial diffusion is less pronounced than on the kinetics of substitutional diffusion. The distribution of "speckles" in the low temperature foils does not show a correlation with the grain boundaries, but rather a "speckle"-free zone of uniform thickness parallel to the surface. This strongly suggests that the influence of grain boundary diffusion on the oxygen ingress into α-Ti is negligible.

At 850°C there is initially a concentration gradient, though this is removed over time (Fig. 11). At 1100°C there should be no concentration gradient, due to a relatively fast diffusion of oxygen in α-Ti, which removes any gradient. At 850 and 1100°C the diffusion of C and O is controlled by diffusion through the outer TiC layer, and diffusion in α-Ti is so fast that apparently no concentration gradient occurs over the core.

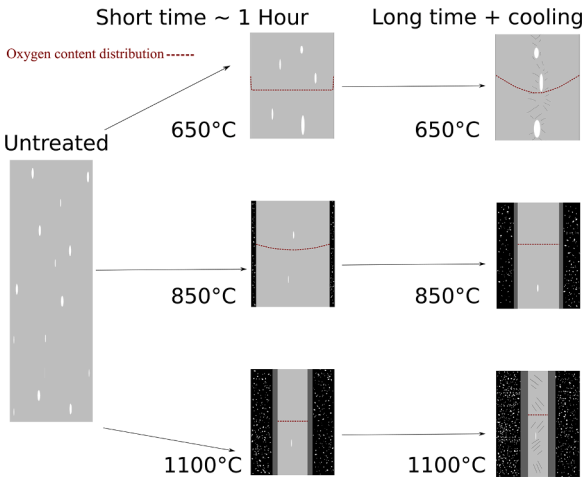

Fig. 11. Schematic growth scenarios for the 650, 850 and 1100°C samples. Growth of an outer TiC layer, an inner TiCO layer, precipitation of TiO in α in 1100°C and localized cooling induced deformation in the 650°C sample. TiC and TiCO are shown as black and gray bars, respectively, while Fe stabilized β is shown in white. Oxygen content in red. Porosities formed in the TiC layer by CO_2 is shown in white.

The origin of porosities in the TiC_x part of the compound layer is at present unknown. They are schematically shown in the TiC_x layer in Fig. 11, with a higher frequency at the grain boundaries. It appears that these porosities develop on conversion of oxygen containing titanium into TiC_x. Since this transformation is associated with a volume increase per Ti atom (cf. Fig. 5), additional densification would be expected. It is suggested here that TiC_x at some distance from the surface does not experience the a_C imposed by the gas mixture and attempts to realize this a_C by partial decomposition. The equilibrium a_C for stabilization of TiC is extremely low [39] and would correspond to a gas ratio $(pCO)^2/pCO_2 < 10^{-6}$ at 1000°C and much lower at lower synthesis temperatures. Then, it could be suggested that in order to realize this ratio and thereby a_C, in particular CO_2 has formed inside the TiC_x layer, preferably at grain boundaries. This hypothesis may be corroborated by the lower O content measured for the highest carbo-oxidation temperature (Fig. 4A). A similar explanation was provided for the development of porosity in iron nitride layers formed in NH_3/H_2 gas mixtures, which form N_2 gas at some distance from the surface to establish the "equilibrium" nitrogen activity [40,41].

5. Conclusions

Gaseous carbo-oxidation of 25-μm-thick grade 2 titanium foils in CO at 600 – 1100°C does not lead to the synthesis of homogeneous foils. The uptake of C and O from the gas is coupled, because equal amounts of C and O are provided by the dissociation of CO at the surface. The resulting carbo-oxidation kinetics depends strongly on the associated microstructure evolution.

At the surface, a thin layer of TiC_x is formed, while O is dissolved in h.c.p. titanium, due to its high solid solubility, particularly in comparison to the very low solid solubility of C. At 600-700°C the overall mass increase by incorporating C and O in the foils depends parabolically on time for the entire carbo-oxidation time and is rate-determined by volume diffusion of O in h.c.p. titanium. The activation energy of the parabolic growth constant is 199 $kJ.mol^{-1}$, consistent with volume diffusion of oxygen in α-Ti. For temperatures up to 850°C, this oxygen

diffusion-controlled overall mass increase applies also for the initial stage of carbo-oxidation. Above 850°C, mass increase appears controlled by the diffusion of species through the TiC_x layer. The associated (apparent) activation energy of 65 $kJ.mol^{-1}$ reflects short circuit diffusion, most likely along grain boundaries in TiC_x. For the stage where O diffusion in h.c.p. titanium is no longer controlling the rate of the overall mass uptake, the oxygen content in TiC_x increases and TiC_xO_y develops at the transition from TiC_x to h.c.p. titanium. The oxygen content in h.c.p. titanium increases with synthesis temperature and first reaches the solubility limit at about 1000°C. Along with reaching oxygen saturation in h.c.p. titanium the TiO phase develops as plates within the foil core. These plates appear oriented along preferred crystallographic orientations. The hardness and indentation modulus of h.c.p. titanium as determined with nanoindentation evolve with temperature and depend linearly on the *c/a* ratio of the hexagonal lattice, which scales with the interstitial content. The hardness and indentation modulus are consistent with the dissolution of only O in h.c.p. titanium.

Data availability

The raw/processed data required to reproduce these findings cannot be shared at this time due to technical or time limitations.

CRediT authorship contribution statement

Frederik Bojsen Kværndrup: Conceptualization, Methodology, Formal analysis, Validation, Investigation, Visualization, Project administration, Writing – original draft, Writing – review & editing. **Kristian V. Dahl:** Conceptualization, Software, Formal analysis, Investigation, Writing – original draft. **Dominique Poquillon:** Investigation, Formal analysis, Resources. **Kenny Ståhl:** Methodology, Investigation, Validation, Resources. **Marcel A.J. Somers:** Conceptualization, Methodology, Formal analysis, Resources, Supervision, Writing – review & editing. **Thomas L. Christiansen:** Funding acquisition, Project administration, Resources, Conceptualization, Methodology, Supervision, Writing – original draft, Writing – review & editing.

Declaration of Competing Interest

The authors declare that they have no known competing financial interests or personal relationships that could have appeared to influence the work reported in this paper.

Acknowledgements

The work has been carried out with financial support from the Danish Council for Independent Research under grant DFF - 7017-00182. We thank Mrs. Sophie Gouy of The Raimond Castaing Microanalysis Centre for the realization of the EPMA analyses.

Supplementary materials

Supplementary material associated with this article can be found, in the online version, at doi:10.1016/j.tca.2021.178991.

References

[1] H.R. Ogden, R.I. Jaffee, The Effects of Carbon, Oxygen, and Nitrogen on the Mechanical Properties of Titanium and Titanium Alloys, 1955, https://doi.org/10.2172/4370612.
[2] D. Gupta, S. Weinig, The dislocation-oxygen interaction in alpha titanium and its effect on the ductile-to-brittle transition, Trans. Am. Inst. Min. Metall. Eng. 215 (1959) 209–216.
[3] H. Conrad, Effect of interstitial solutes on the strength and ductility of titanium, Prog. Mater. Sci. 26 (1981) 123–403, https://doi.org/10.1016/0079-6425(81)90001-3.
[4] Y. Okazaki, E. Gotoh, Comparison of metal release from various metallic biomaterials in vitro, Biomaterials 26 (2005) 11–21, https://doi.org/10.1016/j.biomaterials.2004.02.005.
[5] A. Zhecheva, W. Sha, S. Malinov, A. Long, Enhancing the microstructure and properties of titanium alloys through nitriding and other surface engineering methods, Surf. Coatings Technol. 200 (2005) 2192–2207, https://doi.org/10.1016/j.surfcoat.2004.07.115.
[6] B. Sarma, K.S. Ravi Chandran, Recent advances in surface hardening of titanium, Jom 63 (2011) 85–92, https://doi.org/10.1007/s11837-011-0035-0.
[7] P. Ehrlich, Lösungen von Sauerstoff in metallischem Titan, Zeitschrift Für Anorg. Und Allg. Chemie. 247 (1941) 53–64, https://doi.org/10.1002/zaac.19412470106.
[8] D.J. Maykuth, H.R. Ogden, R.I. Jaffee, Alloys of titanium with carbon, oxygen and nitrogen, J. Met. 188 (1950) 1261–1266.
[9] W.L. Finlay, J.A. Snyder, Effects of three intersitial solutes (N, O and C), J. Met. 188 (1950) 277–286, https://doi.org/10.1017/CBO9781107415324.004.
[10] L. Stone, H. Margolin, Titanium-rich regions of the Ti-C-N, Ti-C-O, and Ti-N-O phase diagrams, J. Met. (1953), https://doi.org/10.15713/ins.mmj.3.
[11] S. Andersson, B. Collen, G. Kruuse, U. Kuylenstierna, A. Magneli, H. Pestmalis, S. Åsbrink, Identification of titanium oxides by x-ray powder patterns, Acta Chem. Scand. (1957).
[12] T. Hurlen, H. Kjollesdal, J. Markali, N. Norman, Oxidation of titanium, Oxidation of Titanium, Central Institute for Industrial Research, (1958).
[13] A. Takamura, Surface hardening of titanium by oxygen, Trans. JIM. 3 (1962) 10–14.
[14] E. Bisogni, G. Mah, C. Wert, Diffusion of gases in special interstitial sites in hafnium, J. Less-Common Met. 7 (1964) 197–204, https://doi.org/10.1016/0022-5088(64)90066-9.
[15] S. Andersson, B. Collen, U. Kuylenstierna, A. Magneli, Phase analysis studies on the titanium-oxygen system, Acta Chem. Scand. (1957).
[16] D. Bandyopadhyay, R. Sharma, N. Chakraborti, The Ti Al C system (titanium - aluminum - carbon), J. Phase Equilibria - J. Phase Equilib. 21 (2000) 195–198, https://doi.org/10.1361/105497100770340273.
[17] J. Vicens, J.-L. Chermant, Contribution a l'etude du systeme titane-carbone-oxygene, Rev. Chim. Miner. 9 (1972) 557–567.
[18] H. Nishimura, H. Kimura, On the equilibrium diagram of titanium-oxygen-carbon system (IV), J. Japan Inst. Met. Japan Inst. Met. Mater. 20 (1956) 589–592, https://doi.org/10.2320/jinstmet1952.20.10_589.
[19] J.L. Murray, H.A. Wriedt, Murray, Wriedt - 1987 - The O−Ti (oxygen-titanium) system, Bull. Alloy Phase Diagrams 8 (1987) 148–165.
[20] V.M. Fedirko, I.M. Pohrelyuk, O.I. Yas'Kiv, Formation of functional coatings based on interstitial compounds on titanium under the conditions of thermodiffusion saturation, Mater. Sci. 42 (2006) 299–308, https://doi.org/10.1007/s11003-006-0083-8.
[21] V. Moisy-Maurice, N. Lorenzelli, C.H. De Novion, P. Convert, High temperature neutron diffraction study of the order-disorder transition in TiC1-x, Acta Metall 30 (1982) 1769–1779, https://doi.org/10.1016/0001-6160(82)90093-1.
[22] T. Christiansen, M.A.J. Somers, Controlled dissolution of colossal quantities of nitrogen in stainless steel, Metall. Mater. Trans. A-Physical Metall. Mater. Sci. 37A (2006) 675–682, https://doi.org/10.1007/s11661-006-0039-5.
[23] J.T. Slycke, E.J. Mittemeijer, M.A.J. Somers, Thermodynamics and Kinetics of Gas and Gas-Solid Reactions, Woodhead Publishing Limited, 2014, https://doi.org/10.1533/9780857096524.1.3.
[24] R.J. Hill, C.J. Howard, A computer program for Rietveld analysis of fixed wavelength X-ray and neutron powder diffraction patterns, Lucas Heights, N.S.W. : Australian Atomic Energy Commission, ISBN: 0642598355, 1986.
[25] M. Dao, N. Chollacoop, K.J. Van Vliet, T.A. Venkatesh, S. Suresh, Computational modeling of the forward and reverse problems in instrumented sharp indentation, Acta Mater 49 (2001) 3899–3918, https://doi.org/10.1016/S1359-6454(01)00295-6.
[26] F.B. Kværndrup, Ö.C. Kücükyildiz, G. Winther, M.A.J. Somers, T.L. Christiansen, Extreme hardening of titanium with colossal interstitial contents of nitrogen and oxygen, Mater. Sci. Eng. A. 813 (2021), 141033.
[27] W.C. Oliver, G.M. Pharr, An improved technique for determining hardness and elastic modulus using load and displacement sensing indentation experiments, J. Mater. Res. 7 (1992) 1564–1583, https://doi.org/10.1557/JMR.1992.1564.
[28] A. Atkinson, Transport processes during the growth of oxide films at elevated temperature, Rev. Mod. Phys. 57 (1985) 437–470, https://doi.org/10.1103/RevModPhys.57.437.
[29] A.N. Christensen, R. Hämäläinen, U. Turpeinen, A.F. Andresen, O. Smidsrød, C.-O. Pontchour, P. Phavanantha, S. Pramatus, B.N. Cyvin, S.J. Cyvin, The temperature factor parameters of some transition metal carbides and nitrides by single crystal X-ray and neutron diffraction, Acta Chem. Scand. 32a (1978) 89–90, https://doi.org/10.3891/acta.chem.scand.32a-0089.
[30] F.B. Kværndrup, M.A.J. Somers, T.L. Christiansen, Extreme Expansion and Reversible Hydrogen Solubility in h.c.p. Titanium Stabilized by Colossal Interstitial Alloying [Submitted], 2021.
[31] R. Traylor, R. Zhang, J. Kacher, J.O. Douglas, P.A.J. Bagot, A.M. Minor, Impurity and texture driven HCP-to-FCC transformations in Ti-X thin films during in situ TEM annealing and FIB milling, Acta Mater 184 (2020) 199–210, https://doi.org/10.1016/j.actamat.2019.11.047.
[32] F.B. Kværndrup, F.B. Grumsen, S. Kadkhodazadeh, K.V. Dahl, M.A.J. Somers, T. L. Christiansen, Diffraction Based Identification of an Elusive FCC Phase in Carbo-Oxidized Titanium, 2021 [Accepted in Materials Characterization].
[33] H. Nakajima, M. Koiwa, Diffusion in Titanium, Bull. Japan Inst. Met. 30 (1991) 526–535, https://doi.org/10.2320/materia1962.30.526.

[34] J.O. Andersson, T. Helander, L. Höglund, P. Shi, B. Sundman, Thermo-Calc & DICTRA, computational tools for materials science, Calphad Comput. Coupling Phase Diagrams Thermochem. 26 (2002) 273–312, https://doi.org/10.1016/S0364-5916(02)00037-8.
[35] F.J.J. Van Loo, W. Wakelkamp, G.F. Bastin, R. Metselaar, Diffusion of carbon in TiC1-y and ZrC1-y, Solid State Ionics. 32–33 (1989) 824–832, https://doi.org/10.1016/0167-2738(89)90364-0.
[36] M.J. Puska, M. Sob, G. Brauer, T. Korhonen, First-principles calculation of positron lifetimes and affnities in perfect and imperfect transition-metal carbides and nitrides, Phys. Rev. B. 49 (1994) 947–957.
[37] M. Schuhmacher, P. Eveno, Oxygen diffusion in titanium carbide, Solid State Ionics 12 (1984) 263–270, https://doi.org/10.1016/0167-2738(84)90155-3.
[38] D.J.J. Maykuth, F.C.C.. Holden, D.N.N. Williams, H.R. Ogden, R.I.I. Jaffee, The Effects of Alloying Elements in Titanium. Volume B. Physical and Chemical Properties, Deformation and Transformation Characteristics, 1961.
[39] S.R. Shatynski, The thermochemistry of transition metal carbides, Oxid. Met. 13 (1979) 105–118, https://doi.org/10.1007/BF00611975.
[40] M.A.J. Somers, N.M. van der Pers, D. Schalkoord, E.J. Mittemeijer, Dependence of the lattice parameter of γ′ iron nitride, Fe4N1−x, on nitrogen content; accuracy of the nitrogen absorption data, Metall. Trans. a (Physical Metall. Mater. Sci. 20A (1989) 1533–1539, https://doi.org/10.1007/BF02665509.
[41] T. Christiansen, M.A.J. Somers, Controlled dissolution of colossal quantities of nitrogen in stainless steel, Metall. Mater. Trans. A Phys. Metall. Mater. Sci. 37 (2006) 675–682, https://doi.org/10.1007/s11661-006-0039-5.